

pubs.acs.org/acsaelm Letter

Coherent Hopping Transport and Giant Negative Magnetoresistance in Epitaxial CsSnBr₃

Liangji Zhang, Isaac King, Kostyantyn Nasyedkin, Pei Chen, Brian Skinner, Richard R. Lunt,* and Johannes Pollanen*



ACCESS

Cite This: https://doi.org/10.1021/acsaelm.1c00409



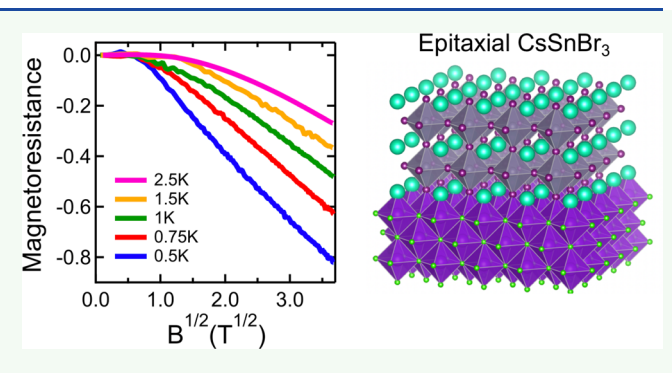
Article Recommendations

ABSTRACT: Single-crystal inorganic halide perovskites are attracting interest for quantum device applications. Here we present low-temperature quantum magnetotransport measurements on thin film devices of epitaxial single-crystal CsSnBr₃, which exhibit two-dimensional Mott variable range hopping (VRH) and giant negative magnetoresistance. These findings are described by a model for quantum interference between different directed hopping paths, and we extract the temperature-dependent hopping length of charge carriers, their localization length, and a lower bound for their phase coherence length of ~100 nm at low temperatures. These observations demonstrate that epitaxial halide

perovskite devices are emerging as a material class for low-

dimensional quantum coherent transport devices.

Metrics & More



s Supporting Information

KEYWORDS: epitaxial halide perovskites, CsSnBr₃, magnetotransport, quantum devices, giant negative magnetoresistance

 $oldsymbol{ extstyle I}$ alide perovskites have emerged over the past decade as a III fundamentally intriguing class of semiconductors with a wide variety of potential applications. These materials have shown remarkable optoelectronic properties including high photoluminescence quantum yields, high optical absorption, long carrier diffusion length, and widely tunable bandgaps.3 These optical and electronic properties make halide perovskites excellent for electronic devices such as light-emitting diodes, semiconductor lasers, and solar cells. To overcome the limitations of grain boundaries and ionic defects common in conventional solution-processed polycrystalline halide perovskite, single-crystal epitaxial growth of halide perovskites has been introduced.⁷⁻¹¹ These new growth techniques also enable the study of delicate quantum properties of charge carriers in halide perovskites in quantum devices and 2D quantum wells.7 Previously, we have reported on the observation of phase coherent transport of charge carriers in the presence of spin—orbit coupling manifesting in weak antilocalization in epitaxial CsSnI₃. Phase coherent quantum interference effects in the form of weak localization have also been recently reported in quasi-epitaxial CsPbBr₃. ¹³ Additionally, hybrid organic-inorganic halide perovskites of singlecrystal MAPbI3 and MAPbBr3 have been shown to exhibit a variety of low-temperature and high-magnetic field transport phenomena under illumination.¹⁴ In this present work we show that coherent transport effects can be realized in another high-quality halide perovskite epitaxial material, namely thin films of CsSnBr₃, at low temperature and high magnetic field.

These effects result from the interference of coherent charge carrier hopping trajectories and manifest in a large device magnetoresistance. In addition to enhancing the fundamental understanding of low-dimensional phenomena in halide perovskites, low-temperature magnetoresistance measurements such as those described in this Letter also provide key insights into the possible transport regimes that can realized in this class of materials. Looking ahead, it will be compelling to investigate which material parameters (e.g., doping, crystal structure, strain, etc.) are involved in transitioning between different transport regimes given that a variety of coherent effects have now been observed. 12-14 This knowledge will impact the material design and development of future quantum electronic devices based on epitaxial halide perovskites.

Two-dimensional (2D) Mott variable range hopping (VRH) is a mechanism for transport in a disordered 2D electron system in which the wave functions of charge carriers tend to localize in the vicinity of lattice defects. At sufficiently low temperature, the electric current in these systems is transported by phonon-assisted tunneling from one localized state to the other, with the dominant hopping processes taking place

Received: May 4, 2021 Accepted: July 8, 2021



between distant rather than nearest-neighboring sites. 15,16 The hopping rate between localization sites leads to Mott's law for conductivity, which in 2D systems is given by $\ln[R(T)] \sim (1/T)^{1/3}$. Many studies have reported that systems in the VRH regime can also show large negative magnetoresistance, including gallium arsenide (GaAs) field-effect transistors, ¹⁷ GaAs/AlGaAs heterostructures, ¹⁸ fluorinated graphene, ¹⁹ Ge films, ²⁰ and In₂O_{3-x} films. ²¹ To explain the negative magnetoresistance, Nguyen, Spivak, and Shkovskii developed a model based on the interference of coherent tunneling trajectories of charge carriers, that is, the so-called NSS model. 22,23 They found that in the VRH regime the quantum interference between distinct forward hopping paths leads to a suppression of the hopping rate between distant sites. Negative magnetoresistance results from the alteration of the relative phase between different hopping paths by the magnetic field, analogous to the effect of weak localization (WL) in the quantum diffusive transport regime. In this paper, we find evidence of this effect in epitaxial CsSnBr₃ thin films. The temperature-dependent resistance of our single-crystal epitaxial CsSnBr₃ system matches well with the 2D Mott VRH, and the giant negative magnetoresistance we observe fits the existing theoretical NSS model predictions. Furthermore, this theoretical model allows us to estimate the various length scales associated with the quantum coherent hopping of charges in this system and place a lower bound on the phase coherence length.

We begin by describing the physics underlying the NSS model and its resemblance to the theory of WL in quantum diffusive transport. In Figure 1 we present a qualitative picture

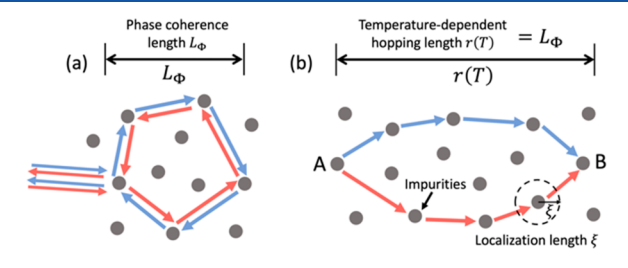


Figure 1. Qualitative picture of two modes of quantum coherent transport in 2D systems. The gray dots represent impurities (sites of elastic scattering). Three different length scales, the phase coherence length L_{Φ} , the temperature-dependent hopping length r(T), and the localization length ξ , are indicated. (a) Model of WL in a conductor. Blue (red) arrows show clockwise (counterclockwise (time-reversed)) diffusive trajectories. (b) VRH and the NSS model in an insulator. A charge carrier tunnels from site A to an energetically favorable site B. The red path and the blue path represent two possible tunneling trajectories, which contribute to the overall hopping amplitude from A to B.

of these two modes of quantum coherent transport. The various relevant length scales, including the temperature-dependent typical hopping length r(T), the charge carrier localization length at zero magnetic field ξ , and the phase coherence length L_{Φ} , are shown in Figure 1 along with their sizes relative to each other.

In the quantum diffusive transport regime, which arises at a higher charge carrier density relative to the VRH regime, the coherence among multiple elastic scattering paths of a single electron can lead to an enhancement of backscattering, as shown in Figure 1a. An externally applied magnetic field introduces relative phase shifts between different scattering

paths and thus leads to negative magnetoresistance, which is the hallmark of WL.²⁴ In analogy to WL, coherent transport also appears at significantly lower charge carrier density in the variable range hopping regime and can be affected by a magnetic field. To understand the magnetoresistance in the hopping regime, the NSS model considers the overall hopping amplitude between two localized sites as the sum of amplitudes of different tunneling trajectories, each of which involves an electron or hole passing virtually through multiple localized impurity states, as depicted in Figure 1b. When an external magnetic field is applied, a phase shift is introduced that can coherently enhance the overall hopping amplitude and lead to a large negative magnetoresistance. ^{25,26} In this work, we present magnetotransport measurements on epitaxial CsSnBr₃ devices demonstrating VRH coherent transport that is consistent with the theoretical description provided by the NSS model.

For these measurements a 30 nm thick epitaxial film of $CsSnBr_3$ was deposited stoichiometrically on a cleaved [100] surface of a sodium chloride (NaCl) single-crystal substrate. The growth of the epitaxial layer was performed at pressures less than 3×10^{-6} Torr and a temperature of 23 °C. The schematic structure of the epilayer and *in situ* real-time reflection high-energy electron diffraction patterns of the grown epilayer are shown in Figure 2. We note that streaks for

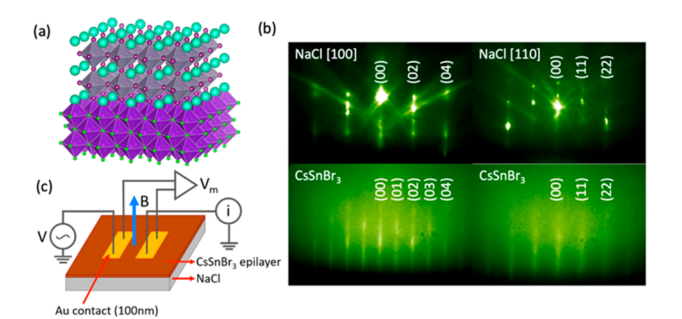


Figure 2. (a) Crystal structure of epitaxial cesium tin bromide (CsSnBr₃) on NaCl (cyan is Cs, gray is Sn, dark purple is Br, green is Na, and purple is Cl). (b) Reflective high-energy electron diffraction (RHEED) pattern of the NaCl substrate (top panels) and CsSnBr₃ thin film showing crystalline streaks in both the NaCl and epitaxially grown CsSnBr3 that vary as expected with rotation. Note the additional (01) streaks emerge for CsSnBr₃ due to the primitive cell versus the face-centered-cubic cell of the substrate. (c) Schematic of the transport measurement setup. These experiments were performed between evaporated gold contacts on 30 nm thick epitaxial CsSnBr₃ thin film device. The device conductivity was calculated from the measured value of the voltage $V_{\rm m}$ and the measured current I, which were obtained by using standard low-frequency AC lock-in. An externally applied magnetic field B applied perpendicular to the plane of the CsSnBr3 epilayer enabled measurement of the magnetotransport at low temperature.

the perovskite layer emerge between the substrate streaks due to the transition from the face-centered cubic structure to a primitive one. After growth, 2.0 mm \times 0.5 mm gold pads (100 nm thick) were electron-beam evaporated onto the CsSnBr $_3$ epilayer to enable standard lock-in-based low-frequency (10 Hz) AC electrical transport measurements (Figure 2). After attaching measurement leads, we loaded devices into a hermetically indium O-ring-sealed copper sample container and thermally anchored to the mixing chamber of a dilution refrigerator for the low temperature ($\sim \! 10$ mK) and high

magnetic field (up to $B = \pm 13.5$) transport measurements. Because of the air-sensitive nature of the samples, devices were kept in an entirely dry, oxygen-free environment during fabrication, wire-up, cooldown, and measurement (see the Supporting Information, section S1).

In Figure 3 we show the resistance of a CsSnBr₃ epitaxial thin film device versus temperature as it is cooled from room

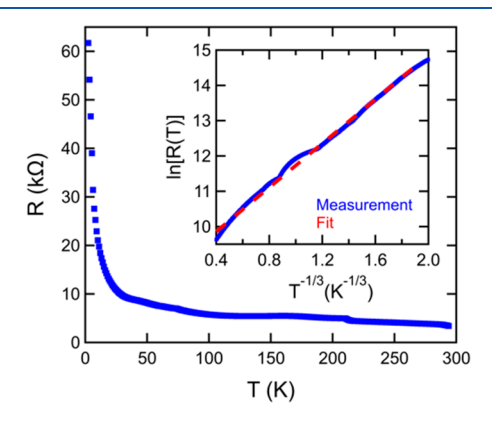


Figure 3. Temperature-dependent resistance of CsSnBr₃ epitaxial thin film at B = 0. Inset: logarithm of the resistance as a function of $T^{-1/3}$. The red line is a fit to the data based on the temperature dependence of 2D Mott VRH transport.

temperature to 2.4 K in the absence of a magnetic field. We observe that the device resistance increases as the temperature decreases and reaches many tens of $k\Omega$ at the lowest temperatures. This change is consistent with that of a lightly doped semiconductor. While previous work has reported ohmic contact between CsSnBr3 and Au at room temperature, 7,27 our two-terminal resistance measurements cannot preclude a contribution from a contact resistance between the evaporated gold and the CsSnBr3 epilayer; however, we emphasize that such a contact resistance would not change the conclusions we draw regarding coherent hopping transport described below. We also note that recent theoretical work has indicated the potential role of electrode induced impurities in CsSnBr₃, which could be investigated with future fourterminal devices. Finally, we note that all measurements reported here were performed in a regime of linear response, which was ensured by performing device IV characteristics at the lowest temperatures.

In the resistance data we observe a repeatable small kink that appears at ~215 K in all of the samples we have measured (see Figure 3 and Supporting Information, section 2). This kink is likely associated with a structural phase transition in the epilayer. In fact, structural phases transitions have been reported previously in bulk CsSnBr₃.²⁹ Moreover, our *in situ* RHEED diffraction measurements on rough CsSnBr₃ show an increase in the c/a lattice ratio of $7 \pm 1\%$ as the sample is cooled from room temperature to 83 K, confirming the presence of a cubic to tetragonal phase transition (see the Supporting Information, section 2).

In the inset of Figure 3, the low-temperature data show the characteristic dependence associated with 2D Mott VRH transport and are well fit to the form of $\ln[R(T)] \sim (T_0/T)^{1/3}$. The characteristic temperature $T_0 = 32$ K is obtained from the slope of the fitted line. The observation of Mott VRH from the CsSnBr₃ epitaxial thin film device indicates that at low temperatures the tunneling

distance of strongly localized charge carriers in $CsSnBr_3$ is much larger than the distance between impurities. The electrons undergo phonon-assisted tunneling through intermediate localized states, as depicted in Figure 1b. As the temperature is increased, we observe the expected crossover from VRH to thermally activated transport, while below roughly 125 mK we observe a saturation of the device resistance that is likely associated with thermal decoupling of the device (see the Supporting Information, section S3).

The coherent interference between hopping transport trajectories can be revealed by performing device resistance measurements under the application of a large magnetic field. In Figure 4 we present results of the low-temperature

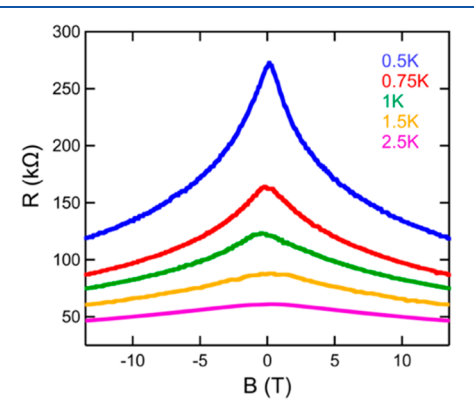


Figure 4. Magnetoresistance of a $CsSnBr_3$ epitaxial thin film at different temperatures. The applied magnetic field is normal to the $CsSnBr_3$ film. The peak of the magnetoresistance weakens as the temperature increases, indicating that the length scale associated with phase-coherent hopping is reduced. We note that the data presented here are from a single device but have been reproduced with additional samples grown separately (see the Supporting Information, section S4).

magnetoresistance measurements on epitaxially grown CsSnBr₃. The measurements were performed at different temperatures with an external magnetic field applied normal to the plane of the epitaxial film. Unlike the negative magnetoresistance often observed in the WL regime, in which the magnetoresistance only varies by a few percent, we observe a giant negative magnetoresistance with no sign of saturation over the full field range ($\pm 13.5 \text{ T}$) at T = 0.5 K with the ratio of R(0)/R(B) significantly exceeding unity. This is consistent with results shown in reports for GaAs/AlGaAs heterojunctions and In_2O_{3-x} films in the VRH regime 18,21 and is consistent with the predictions of the NSS model. We also observe a weakening of the negative magnetoresistance peak as the measurement temperature increases, which could indicate that the length scale associated with phase-coherent hopping is reduced. This could result from increased inelastic scattering from phonons or charge carriers. Alternatively, this weakening could potentially be associated with a contribution from positive (orbital) magnetoresistance as the temperature is increased.

The NSS model also provides a framework for understanding the functional dependence of the magnetoresistance as the temperature is increased, ²⁶ which is given by

$$\ln\left[\frac{R(B)}{R(0)}\right] = -\gamma r(T) \left(\frac{e}{\hbar}\right)^{1/2} B^{1/2} \tag{1}$$

where γ is a numerical coefficient which is estimated to be $0.1/\sqrt{2}$ and r(T) is the temperature-dependent hopping length. In particular, eq 1 predicts a characteristic square-root dependence of $\ln R(B)$, which serves as a fingerprint of the underlying NSS physics. We have plotted the magnetoresistance data in the form of natural logarithm of normalized magnetoresistance $\ln[R(B)/R(0)]$ as a function of $B^{1/2}$ in Figure 5, which clearly demonstrates the expected functional

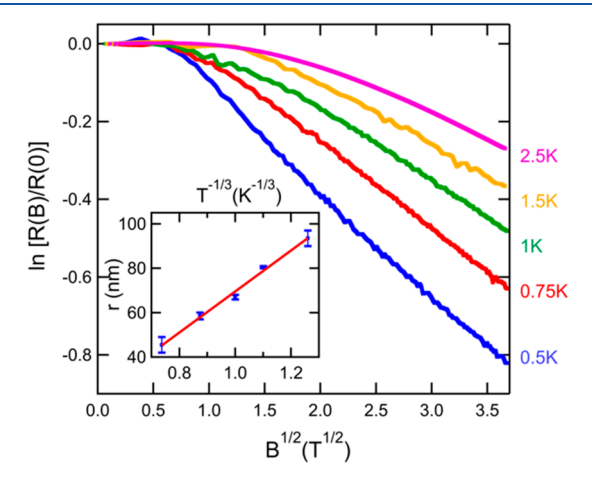


Figure 5. Logarithm of the normalized magnetoresistance $\ln[R(B)/R(0)]$ as a function of the square root of the magnetic field $(B^{1/2})$ at different temperatures as indicated. Inset: temperature-dependent hopping length r(T) as a function of $T^{-1/3}$.

dependence. The temperature-dependent hopping length r(T) can be obtained from the slope of the linear regime in Figure 5 (see eq 1), which yields $r(T)\cong 94$, 81, 67, 59, and 46 nm at 0.5, 0.75, 1, 1.5, and 2.5 K, respectively. In the low-temperature regime of 2D Mott VRH, r(T) should have the following temperature dependence $r(T)\approx \xi(T_0/T)^{1/3}.^{15,16}$ In the inset of Figure 5, we plot r(T) as a function of $T^{-1/3}$, which shows good agreement with this expected behavior for 2D Mott VRH and is independently consistent with our temperature-dependent resistance measurements at zero magnetic field. We also note that the corresponding localization length for charge carriers ξ can be determined from the slope of r(T), from which we find $\xi\approx 30$ nm.

Our measurements and analysis also allow us to place a lower bound on the phase coherence length for charge carriers in CsSnBr₃. In particular, the NSS model is applicable when the phase coherence length L_{Φ} is longer than r(T), as shown in Figure 1b. In this limit the hopping paths retain phase coherence. Equation 1 also requires that the magnetic length $L_B = (\hbar/eB)^{1/2}$ be shorter than the hopping length r(T), so that there are multiple quanta of magnetic flux through a typical closed-loop hopping path, and the magnetic field strongly alters the phase of the charge carrier trajectories. Our observations in aggregate indicate good agreement with the NSS model suggesting that both conditions are fulfilled, and the hierarchy of length scales $L_B \leq r(T) \leq L_{\Phi}$ is achieved. In Figure 5 at T = 0.5 K, we observe linear dependence of $\ln[R(B)/R(0)]$ on $B^{1/2}$ for all values of $B^{1/2} \ge 0.6$ $T^{1/2}$, with a weaker dependence at smaller fields. This high-field regime corresponds to $L_B \leq 40$ nm, and the condition $L_B \le r(T = 0.5 \text{ K})$ is satisfied. While we cannot directly measure the phase coherence length L_{Φ} in the VRH regime, the requirement that L_{Φ} is greater than r(T = 0.5 K) implies a

phase coherence length significantly larger than at least \sim 100 nm. This is consistent with the notably high phase coherence length measured in epitaxial CsSnI₃.¹²

In summary, we have observed giant negative magnetoresistance in single-crystalline epitaxial thin film CsSnBr₃. The devices exhibit a strongly localized 2D Mott VRH of charge carriers. The negative magnetoresistance can be understood within the context of the NSS model, which describes the interference of coherent hopping between localized states. On the basis of this model, we analyze our data to determine the relevant transport length scales including the low-temperature hopping length and the localization length. Additionally, we can place a lower bound on the phase coherence length of ~100 nm for charge carriers in this epitaxial thin film halide perovskite. To our knowledge, these results are the first to demonstrate phase coherent hopping transport and large negative magnetoresistance in halide perovskites. They add to the growing body of evidence demonstrating that epitaxial halide perovskite thin film devices are emerging as an exciting new class of low-dimensional quantum electronic materials. As the quality of epitaxial halide perovskite materials continues to improve via advances in growth, doping, and strain engineering, one can expect the emergence of ever more subtle and exotic electronic states of matter in these materials at low temperatures. For example, future low-dimensional electron systems based on halide perovskites such as CsSnBr₃ could one day provide a novel platform for investigating the collective states in the fractional quantum Hall regime. Additionally, leveraging the advances of halide perovskite epitaxy opens the door for developing high-quality devices exhibiting symmetrybroken interfacial states with unique physical properties (e.g., ferroelectricity, coherent transport, and spin-orbit coupling) not realizable in bulk materials.

ASSOCIATED CONTENT

Supporting Information

The Supporting Information is available free of charge at https://pubs.acs.org/doi/10.1021/acsaelm.1c00409.

CsSnBr₃ device handling details; evidence for a structural phase transition at low temperature; temperature-dependent device transport outside the VRH regime; data for additional device (PDF)

AUTHOR INFORMATION

Corresponding Authors

Richard R. Lunt — Department of Chemical Engineering and Materials Science, Michigan State University, East Lansing, Michigan 48824, United States; orcid.org/0000-0003-4248-6312; Email: rlunt@msu.edu

Johannes Pollanen — Department of Physics and Astronomy, Michigan State University, East Lansing, Michigan 48824, United States; orcid.org/0000-0002-4314-5045; Email: pollanen@msu.edu

Authors

Liangji Zhang — Department of Physics and Astronomy, Michigan State University, East Lansing, Michigan 48824, United States

Isaac King – Department of Chemical Engineering and Materials Science, Michigan State University, East Lansing, Michigan 48824, United States

- Kostyantyn Nasyedkin Department of Physics and Astronomy, Michigan State University, East Lansing, Michigan 48824, United States; Neutron Scattering Division, Oak Ridge National Laboratory, Oak Ridge, Tennessee 37831, United States
- Pei Chen Department of Chemical Engineering and Materials Science, Michigan State University, East Lansing, Michigan 48824, United States
- Brian Skinner Department of Physics, The Ohio State University, Columbus, Ohio 43210, United States

Complete contact information is available at: https://pubs.acs.org/10.1021/acsaelm.1c00409

Notes

The authors declare no competing financial interest.

ACKNOWLEDGMENTS

We thank J. I. A. Li, B. I. Shklovskii, and E. A. Henriksen for fruitful discussions. This work was supported by the National Science Foundation via Grant DMR-1807573. J.P. also acknowledges the valuable support of the Cowen Family Endowment at MSU. B.S. was partially supported by the Center for Emergent Materials, an NSF-funded MRSEC, under Grant DMR-2011876.

REFERENCES

- (1) Huang, J.; Lai, M.; Lin, J.; Yang, P. Rich Chemistry in Inorganic Halide Perovskite Nanostructures. *Adv. Mater.* **2018**, *30* (48), 1802856.
- (2) Hong, K.; Van Le, Q.; Kim, S. Y.; Jang, H. W. Low-Dimensional Halide Perovskites: Review and Issues. *J. Mater. Chem. C* **2018**, *6* (9), 2189–2209.
- (3) Fu, Y.; Zhu, H.; Chen, J.; Hautzinger, M. P.; Zhu, X.-Y.; Jin, S. Metal Halide Perovskite Nanostructures for Optoelectronic Applications and the Study of Physical Properties. *Nat. Rev. Mater.* **2019**, *4* (3), 169–188.
- (4) Zhang, Q.; Tavakoli, M. M.; Gu, L.; Zhang, D.; Tang, L.; Gao, Y.; Guo, J.; Lin, Y.; Leung, S.-F.; Poddar, S.; Fu, Y.; Fan, Z. Efficient Metal Halide Perovskite Light-Emitting Diodes with Significantly Improved Light Extraction on Nanophotonic Substrates. *Nat. Commun.* **2019**, *10* (1), 1–9.
- (5) Cegielski, P. J.; Giesecke, A. L.; Neutzner, S.; Porschatis, C.; Gandini, M.; Schall, D.; Perini, C. A. R.; Bolten, J.; Suckow, S.; Kataria, S.; Chmielak, B.; Wahlbrink, T.; Petrozza, A.; Lemme, M. C. Monolithically Integrated Perovskite Semiconductor Lasers on Silicon Photonic Chips by Scalable Top-down Fabrication. *Nano Lett.* **2018**, *18* (11), 6915–6923.
- (6) Nam, J. K.; Chai, S. U.; Cha, W.; Choi, Y. J.; Kim, W.; Jung, M. S.; Kwon, J.; Kim, D.; Park, J. H. Potassium Incorporation for Enhanced Performance and Stability of Fully Inorganic Cesium Lead Halide Perovskite Solar Cells. *Nano Lett.* **2017**, *17* (3), 2028–2033.
- (7) Wang, L.; Chen, P.; Thongprong, N.; Young, M.; Kuttipillai, P. S.; Jiang, C.; Zhang, P.; Sun, K.; Duxbury, P. M.; Lunt, R. R. Unlocking the Single-Domain Epitaxy of Halide Perovskites. *Adv. Mater. Interfaces* **2017**, *4* (22), 1701003.
- (8) Wang, Y.; Sun, X.; Chen, Z.; Sun, Y.-Y.; Zhang, S.; Lu, T.-M.; Wertz, E.; Shi, J. High-Temperature Ionic Epitaxy of Halide Perovskite Thin Film and the Hidden Carrier Dynamics. *Adv. Mater.* **2017**, 29 (35), 1702643.
- (9) Chen, J.; Morrow, D. J.; Fu, Y.; Zheng, W.; Zhao, Y.; Dang, L.; Stolt, M. J.; Kohler, D. D.; Wang, X.; Czech, K. J.; Hautzinger, M. P.; Shen, S.; Guo, L.; Pan, A.; Wright, J. C.; Jin, S. Single-Crystal Thin Films of Cesium Lead Bromide Perovskite Epitaxially Grown on Metal Oxide Perovskite (SrTiO₃). *J. Am. Chem. Soc.* **2017**, *139* (38), 13525–13532.

- (10) Wang, L.; Chen, P.; Kuttipillai, P. S.; King, I.; Staples, R.; Sun, K.; Lunt, R. R. Epitaxial Stabilization of Tetragonal Cesium Tin Iodide. *ACS Appl. Mater. Interfaces* **2019**, *11* (35), 32076–32083.
- (11) Wang, L.; King, I.; Chen, P.; Bates, M.; Lunt, R. R. Epitaxial and Quasiepitaxial Growth of Halide Perovskites: New Routes to High End Optoelectronics. *APL Mater.* **2020**, *8* (10), 100904.
- (12) Nasyedkin, K.; King, I.; Zhang, L.; Chen, P.; Wang, L.; Staples, R. J.; Lunt, R. R.; Pollanen, J. Extraordinary Phase Coherence Length in Epitaxial Halide Perovskites. arXiv Preprint, https://arxiv.org/abs/2009.05170, 2020; pp 1–18.
- (13) Wang, Y.; Wan, Z.; Qian, Q.; Liu, Y.; Kang, Z.; Fan, Z.; Wang, P.; Wang, Y.; Li, C.; Jia, C.; Lin, Z.; Guo, J.; Shakir, I.; Goorsky, M.; Duan, X.; Zhang, Y.; Huang, Y.; Duan, X. Probing Photoelectrical Transport in Lead Halide Perovskites with van Der Waals Contacts. *Nat. Nanotechnol.* **2020**, 1–8.
- (14) Keshavarz, M.; Wiedmann, S.; Yuan, H.; Debroye, E.; Roeffaers, M.; Hofkens, J. Light-and Temperature-Modulated Magneto-Transport in Organic-Inorganic Lead Halide Perovskites. ACS Energy Lett. 2018, 3 (1), 39–45.
- (15) Shklovskii, B. I.; Efros, A. L. Electronic Properties of Doped Semiconductors; Springer Science & Business Media: 2013; Vol. 45.
- (16) Mott, N. F. Conduction in Glasses Containing Transition Metal Ions. J. Non-Cryst. Solids 1968, 1 (1), 1–17.
- (17) Laiko, E. I.; Orlov, A. O.; Savchenko, A. K.; Il'ichev, E. A.; Poltoratskii, E. A. Negative Magnetoresistance and Oscillations of the Hopping Conductance of a Short N-Type Channel in a GaAs Field-Effect Transistor. *JETP Lett.* 1987, 66, 1258.
- (18) Jiang, H. W.; Johnson, C. E.; Wang, K. L. Giant Negative Magnetoresistance of a Degenerate Two-Dimensional Electron Gas in the Variable-Range-Hopping Regime. *Phys. Rev. B: Condens. Matter Mater. Phys.* 1992, 46 (19), 12830.
- (19) Hong, X.; Cheng, S.-H.; Herding, C.; Zhu, J. Colossal Negative Magnetoresistance in Dilute Fluorinated Graphene. *Phys. Rev. B: Condens. Matter Mater. Phys.* **2011**, 83 (8), 85410.
- (20) Mitin, V. F.; Dugaev, V. K.; Ihas, G. G. Large Negative Magnetoresistance in Ge Films at Ultralow Temperatures and Low Magnetic Fields. *Appl. Phys. Lett.* **2007**, *91* (20), 202107.
- (21) Milliken, F. P.; Ovadyahu, Z. Observation of Conductance Fluctuations in Large In₂O_{3-x} Films. *Phys. Rev. Lett.* **1990**, *65* (7), 911.
- (22) Nguen, V. L.; Spivak, B. Z.; Shkovskii, B. I. Tunnel Hopping in Disordered Systems. Sov. Phys. JETP 1985, 89, 1770–1784.
- (23) Ioffe, L. B.; Spivak, B. Z. Giant Magnetoresistance in the Variable-Range Hopping Regime. *J. Exp. Theor. Phys.* **2013**, *117* (3), 551–569.
- (24) Bergmann, G. Weak Localization in Thin Films: A Time-of-Flight Experiment with Conduction Electrons. *Phys. Rep.* **1984**, *107* (1), 1–58.
- (25) Shklovskii, B. I.; Spivak, B. Z. Scattering and Interference Effects in Variable Range Hopping. *Hopping Transp. solids* **1991**, 28, 271.
- (26) Zhao, H. L.; Spivak, B. Z.; Gelfand, M. P.; Feng, S. Negative Magnetoresistance in Variable-Range-Hopping Conduction. *Phys. Rev. B: Condens. Matter Mater. Phys.* **1991**, 44 (19), 10760.
- (27) Long, R.; Li, B.; Mi, Q. Selection of Contact Materials to P-Type Halide Perovskite by Electronegativity Matching. *AIP Adv.* **2020**, *10* (6), 065224.
- (28) Liang, Y.; Cui, X.; Li, F.; Stampfl, C.; Ringer, S. P.; Zheng, R. Electrode-Induced Impurities in Tin Halide Perovskite Solar Cell Material CsSnBr₃ from First Principles. *npj Comput. Mater.* **2021**, 7 (1), 1–9.
- (29) Mori, M.; Saito, H. An X-Ray Study of Successive Phase Transitions in CsSnBr₃. J. Phys. C: Solid State Phys. 1986, 19 (14), 2391.
- (30) Mott, N. F.; Davis, E. A. Electronic Processes in Non-Crystalline Materials; Oxford University Press: 2012.